Wind and Structures, Vol. 12, No. 6 (2009) 519-540
DOI: http://dx.doi.org/10.12989/was.2009.12.6.519

Experimental and numerical identification of flutter derivatives for nine bridge deck sections

Uwe Starossek* and Hasan Aslan

Hamburg University of Technology, 21073 Hamburg, Germany

Lydia Thiesemann

WTM Engineers, Ballindamm 17, 20095 Hamburg, Germany

(Received February 25, 2009, Accepted July 16, 2009)

Abstract. This paper presents the results of a study into experimental and numerical methods for the identification of bridge deck flutter derivatives. Nine bridge deck sections were investigated in a water tunnel in order to create an empirical reference set for numerical investigations. The same sections, plus a wide range of further sections, were studied numerically using a commercially available CFD code. The experimental and numerical results were compared with respect to accuracy, sensitivity, and practical suitability. Furthermore, the relevance of the effective angle of attack, the possible assessment of non-critical vibrations, and the formulation of lateral vibrations were studied. Selected results are presented in this paper. The full set of raw data is available online to provide researchers and engineers with a comprehensive benchmarking tool.

Keywords: bridge flutter; flutter derivatives; water tunnel; CFD; numerical simulation; effective angle of attack; non-critical vibration; lateral vibration.

1. Introduction

The assessment of the aerodynamic behaviour of a bridge structure is indispensable for long-span bridge design projects. The collapse of the Old Tacoma Narrows Bridge (USA 1940) under a relatively low wind speed highlighted the importance of sound aerodynamic design against bridge flutter–a self-induced periodic motion with divergent amplitudes leading to the destruction of the structure that occurs when the critical wind speed is exceeded. For the determination of the critical wind speed, the standard practice is to undertake a small-scale wind tunnel test either on a sectional or a full model as this method has been proven to yield accurate results. However, wind tunnel tests are costly both in time and financial terms. Accurate preparation of the model is a time-consuming exercise and ad-hoc changes by the design engineer are not easy to implement. Thus, a wind tunnel test usually concludes a near-finished design and ideally confirms the aerodynamic stability of the structure.

* Professor, Corresponding Author, E-mail: starossek@tuhh.de

This leaves the design engineer with the problem of ensuring a good estimate of the aerodynamic behaviour right from the beginning in order not to jeopardize the design schedule and, consequently, the project programme and budget. Therefore, the engineer requires an office-based solution which is practical with respect to time, cost and accuracy to be able to assess the aerodynamic behaviour of the structure for preliminary or optional studies at an early stage of the project. One such solution could lie in Computational Fluid Dynamics (CFD). Due to recent developments in software and hardware, CFD is becoming increasingly popular among design engineers and could well pose an attractive alternative to wind tunnel testing if it delivers reliable results.

This paper presents the results of a study into experimental and numerical methods for the assessment of the aerodynamic behaviour of long-span bridge decks. Experiments in a water tunnel were performed on nine different sections to provide benchmark results for the numerical investigations. All nine sections and further twentytwo sections were analysed using a commercially available CFD code, which is based on the Finite Volume Method. An algorithm was devised to perform the CFD analysis and to obtain the flutter derivatives and the critical wind speed. These results, together with analytically derived ones, are compared for accuracy, sensitivity and practical suitability.

Furthermore, investigations into the effective angle of attack, pre- and post-critical vibrations (where the assumption of harmonic vibrations is not valid), and the effect and formulation of lateral vibrations were undertaken. The widely publicised linear approach of the latter is questioned with the results obtained in this study.

2. Theoretical background

Flutter is considered to be a dynamic stability problem. At the stability border, when the flow velocity is equal to the critical wind speed for flutter, the sum of structural and aerodynamic damping is zero; hence, the structure vibrates in a harmonic motion with constant amplitude. For a section with two degrees of freedom, vertical translation h and rotation α around the longitudinal axis (Fig. 1), the equation of motion can be written as:

$$\mathbf{M}\ddot{\mathbf{x}}(t) + \mathbf{K}\mathbf{x}(t) = \mathbf{F}_L(t) \tag{1}$$

$$\text{with } \mathbf{x}(t) = \begin{bmatrix} h(t) \\ \alpha(t) \end{bmatrix} \text{ and } \mathbf{F}_L(t) = \begin{bmatrix} L(t) \\ M(t) \end{bmatrix}$$

$\mathbf{M}$ and $\mathbf{K}$ are the mass and stiffness matrices, $\mathbf{x}(t)$is the displacement vector and $\mathbf{F}_L(t)$ is the vector of the aerodynamic lift and moment forces.

The formulation of the motion-induced aerodynamic forces $L(t)$ and $M(t)$ can be based on Theodorsen's (1935) aerofoil flutter theory. Several modified expressions exists, either in real or complex notation. The popular real-number expressions (Simiu and Scanlan 1996) read

$$L = \frac{1}{2}\rho u^2 B\left(KH_1^*\frac{\dot{h}}{u} + KH_2^*\frac{B\dot{\alpha}}{u} + K^2H_3^*\alpha + K^2H_4^*\frac{h}{B}\right) \tag{2}$$

$$M = \frac{1}{2}\rho u^2 B\left(KA_1^*\frac{\dot{h}}{u} + KA_2^*\frac{B\dot{\alpha}}{u} + K^2A_3^*\alpha + K^2A_4^*\frac{h}{B}\right) \tag{3}$$

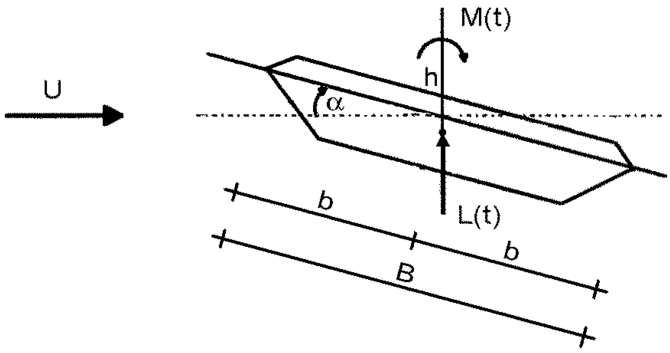

Fig. 1 Two degree of freedom system

where ρ = density of fluid; u = wind speed, B = width of the section, h = vertical displacement, and α = rotational displacement. The eight coefficients H_j^*, A_j^* are the flutter derivatives to be determined either experimentally, numerically, or analytically and are functions of the reduced frequency $K = \omega B/u$, with ω as the circular frequency of motion of the aeroelastic structure. It can be seen that L and M are functions of u and K.

The more compact and mathematically elegant complex number expressions (Starossek 1992, 1993, 1998) read

$$L = \omega^2 \pi \rho b^2 (c_{hh} h + b c_{h\alpha} \alpha) \tag{4}$$

$$M = \omega^2 \pi \rho b^2 (b c_{\alpha h} h + b^2 c_{\alpha\alpha} \alpha) \tag{5}$$

where $b = B/2$ (for conformity with Theodorsen's original notation instead of B). The four complex coefficients c_{mn} are the flutter derivatives in this notation; they are functions of the reduced frequency $k = \omega b/u$. L and M now directly depend on k and ω, which is advantageous for the solution of the resulting eigenvalue problem. For a flat plate, the flutter derivatives can analytically be derived from potential flow theory and read

$$c_{hh} = 1 - \frac{2i}{k} C \tag{6}$$

$$c_{h\alpha} = -\frac{1}{k}\left[i(C+1) + \frac{2}{k} C \right] \tag{7}$$

$$c_{\alpha h} = \frac{i}{k} C \tag{8}$$

$$c_{\alpha\alpha} = \frac{i}{2k}(C-1) + \frac{1}{k^2} C + \frac{1}{8} \tag{9}$$

where C is the Theodorsen function.

The eight coefficients H_j^*, A_j^* of the real notation and the equivalent four coefficients c_{mn} of the complex notation directly relate to each other. The following relationship between complex and real notation exists:

$$c_{hh} \equiv \frac{2}{\pi}(H_4^* + iH_1^*) \tag{10}$$

$$c_{h\alpha} \equiv \frac{4}{\pi}(H_3^* + iH_2^*) \tag{11}$$

$$c_{\alpha h} \equiv \frac{4}{\pi}(A_4^* + iA_1^*) \tag{12}$$

$$c_{\alpha\alpha} \equiv \frac{8}{\pi}(A_3^* + iA_2^*) \tag{13}$$

It is therefore possible to convert one notation into the other.

The critical wind speed for flutter can be calculated based on the flutter derivatives in a dynamic structural analysis either with a simplified two-degree-of-freedom (2-DOF) algorithm or with a more precise Finite Element (FE) calculation as shown by Starossek (1992, 1993).

3. Experiments

The original aim of this study was to assess the reliability of a CFD method for predicting bridge deck flutter. A meaningful assessment requires the direct comparison of the CFD method with a proven method using the same sectional data under the same conditions, as far as practically possible. The current practise is to perform a wind tunnel test either on a small-scale full aeroelastic model or on a sectional model for an accurate investigation of the aerodynamic behaviour. Instead of a wind tunnel, a water tunnel can also be used, especially if only sectional models are to be tested. Water tunnels are not widely used as they are more expensive to maintain and not as flexible as wind tunnels. They do have the advantage, however, of using lower stream velocities due to the higher viscosity of water compared to air and generating relatively large fluid forces. Thus, observations, especially of nonlinear behaviour, and data reading can be more accurate.

The experiments were undertaken in a 1.5 m wide and 0.8 m deep water tunnel of Goettingen type at the University of Stuttgart. The objective of the tests was to determine the static coefficients and the flutter derivatives for a range of bridge deck sections. Furthermore, the effect of various Reynolds numbers and motion amplitudes on the flutter derivatives were assessed.

From the 31 sections which were numerically investigated, nine were chosen for testing (Fig. 2). The selection was based on shape variation and shape popularity in practice (except sections P and R). The availability of previous results from other researchers also played a role in choosing the sections as that allowed for comparison and evaluation of own test results. For section GB, wind tunnel experiments as well as numerical simulations were undertaken, for example, by Walther (1994), Reinhold, *et al.* (1992), Larsen and Jacobsen (1992). Section M was analysed numerically by Morgenthal (2002) and experimentally by Flamand, *et al.* (2001). Experimental results are available for section S from Wienand (1994), and for section R from Hortmanns (1997). Larsen and Walther (1998) analysed the TC section numerically whereas Scanlan and Tomko (1971) undertook wind tunnel testing for the same section. Section G was chosen for investigation as open or slotted sections seem to be the most aerodynamically stable sections for very long bridges Larsen and Astiz (1998).

All section models were 200 mm wide and 490 mm long and had a relatively smooth surface. Sections thicker than 20 mm were made of glass-fibre-composite materials with a brass spine. The

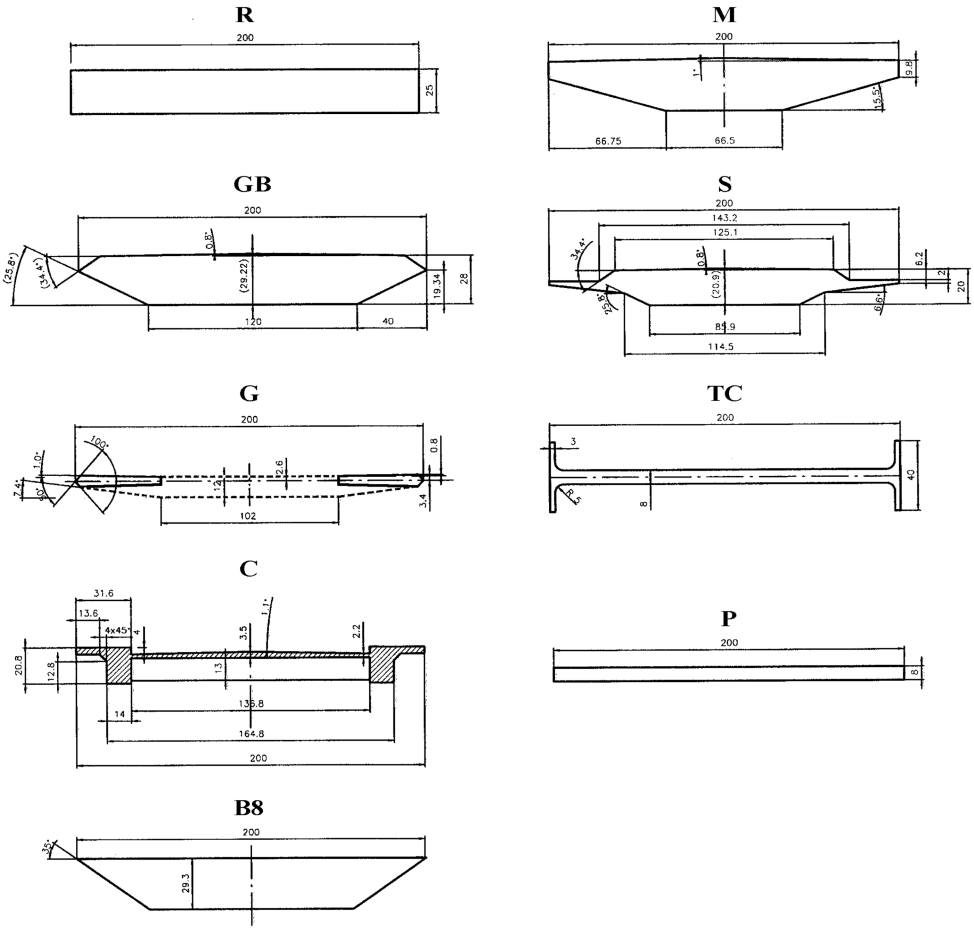

Fig. 2 Sections tested in water tunnel

more complex sections G and C were cut from aluminium; the thin sections P and TC were made of carbon- and glass-fibre composite materials. They were fixed to the rig by special clamps. End plates were attached to all sections to channel the flow in a two-dimensional manner.

The sectional models were suspended from a force balance system and completely submerged in the fluid. The static drag, lift, and moment coefficients were measured for an angle of attack from $\alpha = -10^{o}$ to $\alpha = +10^{o}$ in 1^{o} increments. For measuring the flutter derivatives, the sectional models were forced to move separately in a vertical or a rotational direction in a constant-amplitude harmonic motion.

The tests were undertaken for a range of frequencies, namely from 0.3 Hz to 3 Hz in 0.15 Hz increments. Only for the vertical motions, the frequency was capped at 2 Hz due to maximum allowable acceleration. For the thin section P, the frequency was even limited to 1.5 Hz as higher frequencies could have caused the section to break. To assess the sensitivity of the results on the motion amplitudes, three different amplitudes were chosen. The vertical amplitudes were 2 mm, 4 mm, and 8 mm. Hence, the maximum amplitude was 4% of the width B. The selected rotational amplitudes were 2^{o}, 5^{o}, and 8^{o}. To assess a possible Reynolds number dependency of the results,

the velocity of the stream was also varied. The tests were run with velocities of 0.5 m/s, 0.75 m/s, 1 m/s, and 1.25 m/s. Hence, for a section having a width of $B = 200$ mm, the Reynolds number was between 100,000 and 250,000. Only section GB was tested under different stream velocities (0.5 m/s, 0.7 m/s, 1 m/s, and 1.3 m/s) but since no Reynolds number dependency was visible, the tests were not repeated with the new set of velocities. The turbulence intensity of the stream was less than 1%.

For reliable data acquisition, the readings were passed through a 10 Hz low-pass filter in order to eliminate high-frequency turbulence before recording. However, this resulted in a phase shift which had to be corrected according to the transfer function of the filter. They were then used to identify the flutter derivatives using Fourier analysis (FFT) but not before reducing the measured forces by the inertial of forces of the system measured in air.

The flutter derivatives for section GB matched the ones from Reinhold, *et al.* (1992) reasonably well (Fig. 5), except for the real part $c'_{hh}(H_4^*)$ which showed an offset between the two results. This is probably because Reinhold did not take the virtual mass of the air into account.

The test results regarding a possible Reynolds number or amplitude dependency are shown in Tables 2 and 3, respectively. The sections P and TC are affected the least from the variation of the

Table 1 Four structural data sets

		1	2	3	4
b	[m]	5.95	15.5	15.5	30
ω_h	[1/s]	0.84	0.62	0.622	0.383
ω_α	[1/s]	1.11	1.17	1.71	0.509
ε	[-]	1.32	1.88	2.76	1.33
μ_m	[-]	61.0	19.7	24.1	6.5
r	[-]	0.77	0.71	0.67	1.2
m	[kg/m]	8500	17800	22740	39500
θ	[kg m^2/m]	177730	2173000	2470000	26700000
ξ_h	[-]	0	0	0.002	0.003
ξ_a	[-]	0	0	0.002	0.0015

Table 2 Reynolds number dependency of critical wind speed based on data set 2

Section	Mean wind speed	Standard deviation
	[m/s]	[m/s]
GB	40.34	2.20
S	43.29	2.06
M	39.57	1.59
B8	36.31	2.69
P	37.87	0.32
R	29.60	3.50
G	73.79	2.39
C	23.33	2.01
TC	18.89	0.33

Table 3 Amplitude dependency of critical wind speed based on data set 2

Section	Mean wind speed	Standard deviation
	[m/s]	[m/s]
GB	41.22	0.08
S	42.48	0.10
M	39.34	0.38
B8	37.69	0.17
P	37.77	0.89
R	34.27	1.36
G	76.60	1.67
C	21.23	1.15
TC	16.17	1.89

Reynolds number. All other sections have a standard deviation for the critical wind speed of less than 5%, except section R which was about 10%. The influence of the amplitudes are even smaller for all sections. Only for section TC was the standard deviation for the critical wind speed slightly greater than 10%.

For the comparison with the numerical results, the tests were conducted with a Reynolds number of 200,000, a vertical amplitude of 0.04 B and a rotational amplitude of 5°. The comparison is discussed in Section 5.1.

The full set of experimental results including the raw data for all investigated sections is available online (Starossek 2009).

4. Numerical simulations

Numerical simulations of aerodynamic behaviour of bridge sections to identify flutter derivatives require large computational resources. This is due to the fact that not only a fine spatial but also a fine temporal discretisation is necessary for obtaining acceptable results. With the rapid development of computer hardware, CFD simulations became feasible within the bridge engineering sector. Walther (1994) calculated flutter derivatives with an algorithm based on the grid-free Discrete Vortex (DV) method. The same method was used by Larsen and Walther (1998) to simulate flow over five generic bridge deck sections. Later, the algorithm was adapted by Morgenthal (2002) for high-resolution simulations.

Besides the DV method, the main technique is the grid based Finite Volume (FV) method. Especially with commercial CFD software, the FV method is popular as it can be used for a wide range of applications in various engineering fields such as aerospace, chemical, mechanical, and as civil engineering, to name but a few. This is due to its numerical robustness in the case of irregular meshes. The Navier-Stokes-Equations, which formulate the motion of a fluid substance, are solved for each volumetric element into which the domain is divided.

In this study, the numerical simulations were carried out with the commercial CFD software application COMET, which is based on the Finite Volume method (Thiesemann and Starossek 2002, Thiesemann 2007). The simulations are based on the following assumptions:

(1) 2 degrees of freedom of the section
(2) 2-D laminar flow, no turbulence
(3) incompressible fluid
(4) sinusoidal motion of deck
(5) uniform velocity in the far field
(6) zero velocity at deck wall parallel to surface

The finite volume grid was set up as a structured mesh with about 30,000 two-dimensional control volumes (Fig. 3). Near the deck surface, the grid was progressively refined based on velocity errors obtained after several preliminary runs. The smallest element size along the profile section was 2.5 mm. This fine discretisation extended through the boundary layer and then became coarser with increasing distance to the section. The boundary layer was determined at the far end of the section (1 m) as 11 mm for smooth flow and 33 mm for turbulent flow for a Reynolds number of 200,000. The domain was 5 m long with the section placed within the first third to allow for proper wake formation behind the section. The flow speed was kept constant and the motion frequency was varied within a range of $0 < k < 1$ in 0.1 increments in order to obtain a fine resolution within the critical range.

To model the sinusoidal motion of the deck, the whole grid was moved separately in each of the two degrees of freedom (translational movement normal to the free stream and rotational movement causing periodic change of the angle of attack). The movement was controlled through a command file within COMET. The amplitude of the motion was restricted to $h/b = 0.05$ and $\alpha = 5^{\circ}$. One

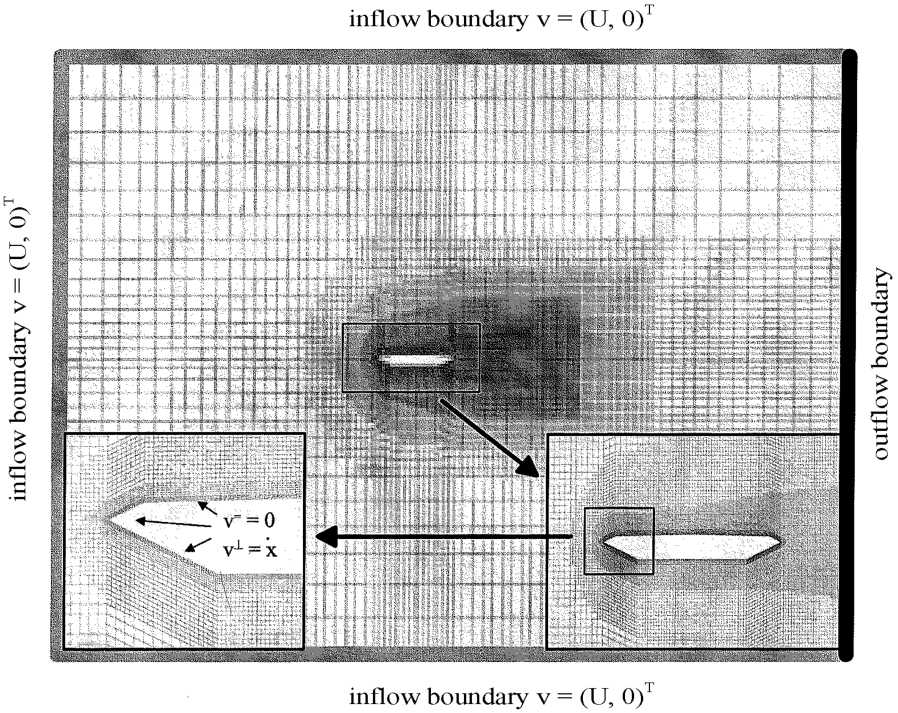

Fig. 3 Boundary conditions of numerical model

period of movement was divided into 3000-5000 time steps (the average time step was 0.0025 s) which ensured that the Courant number was less than unity - an indication for adequate accuracy and reduced numerical dispersion.

The grid movement and the integration of the pressure distribution had to be performed for each time step. The time plots of $L(h)$, $L(\alpha)$, $M(h)$, and $M(\alpha)$ were transformed into the frequency domain with the Fast Fourier method to obtain the flutter derivatives c_{mn}. The results were plotted against the reduced wind speed with intermediate values being approximated by linear interpolation.

As said before, the critical wind speed for flutter can be calculated with a simplified 2-DOF algorithm or with a FE calculation. Coupled CFD-structural time-step analyses taking into account all aerodynamic and structural non-linearities are also possible due to new developments in interface protocols, e.g. MpCCI by the Frauenhofer Institute (2008), between CFD and FE programs. The advantage of such Fluid-Structure-Interaction (FSI) analysis is the accurate simulation of critical and non-critical vibrations in the time domain, that is, the aerodynamic performance of the structure can be assessed not only at the ultimate limit state but also for serviceability (e.g. for vortex shedding, buffeting). Due to high computational costs, however, these analyses are at present limited to systems with small numbers of degrees of freedom.

5. Results

5.1. Comparison of results

All nine sections tested in the water tunnel plus a further 22 bridge deck sections were analysed with the CFD and the analytical (Theodorsen) method. This allowed for the collation an extensive set of results for a wide range of sections with their specific aerodynamic behaviours. Using the same input data, as far as practically possible, for each of the three methods (analytical, experimental, and numerical) allowed a direct comparison of the methods and the aerodynamic behaviour of the sections. The flutter derivative charts, the reduced frequency at flutter onset and the critical wind speed for flutter for various structural properties are directly compared.

The experimental data showed that the variation of the Reynolds number between 100,000 to 250,000 did not greatly influence the results. The results shown and compared here are for a Reynolds number of 200,000 for both the numerical and the experimental tests. Flutter derivatives from the experimental tests are for $Re = 200{,}000$, $h = 0.04B$ and $\alpha = 5^{o}$.

Figs. 5 and 6 show the flutter derivatives obtained from the experiments with the GB section and the M section, respectively. They are given in complex notation. The equivalent results in real notation can be found in (Starossek 2009).

Experimentally determined flutter derivatives $c_{\alpha\alpha}$ for a few selected sections can be compared in Fig. 7. The imaginary part turns positive at particular reduced wind speeds $U_{red} = \frac{\pi}{k}$ for sections TC, C, and R. This is an indication of pure torsional flutter which usually occurs with bluff sections. The derivatives for G and P behave close to the ones of a flat plate. Hence, these profiles can be considered as streamlined sections.

The flutter derivatives obtained from the CFD analysis are compared with those from the water tunnel testing for the sections GB and M in Figs. 8 and 9, respectively (where $c_{mn} = c'_{mn} + ic''_{mn}$).

Based on these flutter derivatives, the critical wind speeds were calculated with an analytical 2-

DOF algorithm using the four different structural data sets assembled in Table 1 (ω_h and ω_α are the circular eigenfrequencies in h and α of the undamped system in vacuum, $\varepsilon = \frac{\omega_\alpha}{\omega_h}$ is the frequency ratio, $\mu = \frac{m}{\pi\rho b^2}$ is the reduced mass, $r = \frac{1}{b}\sqrt{\frac{\theta}{m}}$ is the reduced radius of gyration, m and θ are the mass and the mass moment of inertia per unit length, and ξ_h and ξ_α are the respective damping ratios-to-critical). The results are tabulated in Table 4. For sake of comparison, the theoretical solutions for the flat plate are also presented.

The streamlined section GB has critical wind speeds close to the flat plate for all four structural data sets except for data set 4, for which the difference is greater than 20%. The numerical results are in close agreement with the experimental ones. In addition to the experimentally analysed trapezoidal sections (GB, S, M, B8), a number of variations were numerically investigated (Fig. 4). All sections displayed a critical wind speed within 20% of the theoretical critical wind speed for a thin plate. The results also match previously published results from other researchers (Table 6). Larsen and Jacobsen (1992) had experimentally tested several trapezoidal sections for the design of the Great Belt crossing and compared the critical wind speed with the theoretical ones obtained with the Selberg formula.

A discrepancy between own and others results are found for section M. Flamand, *et al*. (2001) and Morgenthal (2002) had analysed the section and found it prone to torsional flutter. According to their investigations, the reduced wind speed at which the derivative $c''_{\alpha\alpha}$ changes sign was close to the one of section TC. This contradicts the experimentally and numerically determined results in this paper which are similar to the one of a flat plate. A section similar to B8 was found by Scanlan and Tomko (1971) to be prone to torsional flutter. The discrepancy with the results here could be due to a different slenderness of the analysed sections.

A number of trapezoidal sections with fairings were also analysed. In general, additional fairings

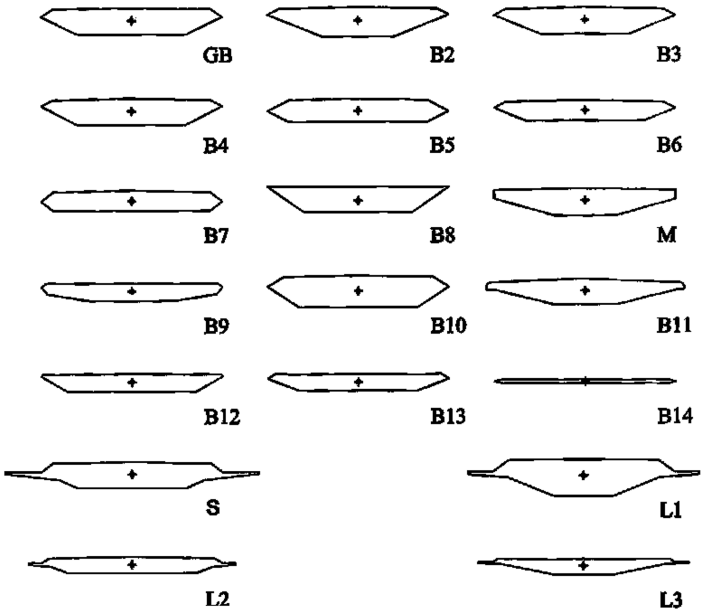

Fig. 4 Numerically investigated trapezoidal sections

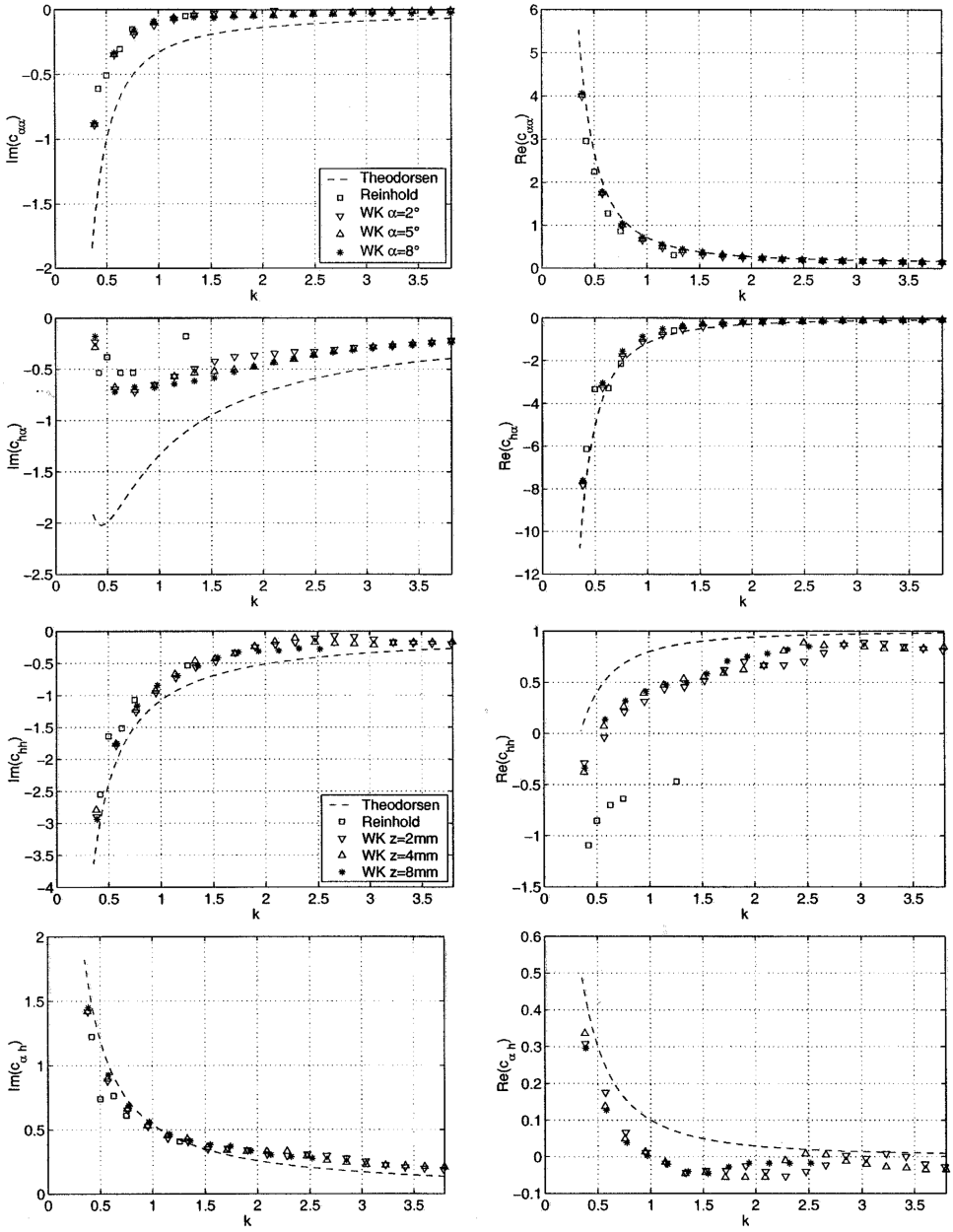

Fig. 5 Flutter derivatives for section GB from water tunnel measurements

improved the critical wind speed by 5 to 10%. The experimentally determined critical wind speeds for section S are close to the theoretical values. However, the numerically determined results overestimate the critical wind speed significantly, especially for data set 4.

The rectangular sections P and R exhibit distinctly different flutter behaviours. Section P is slender and can be classified as a plate-like section, hence, the flutter derivative curves match the analytically derived ones closely. There is also little discrepancy between the numerical and

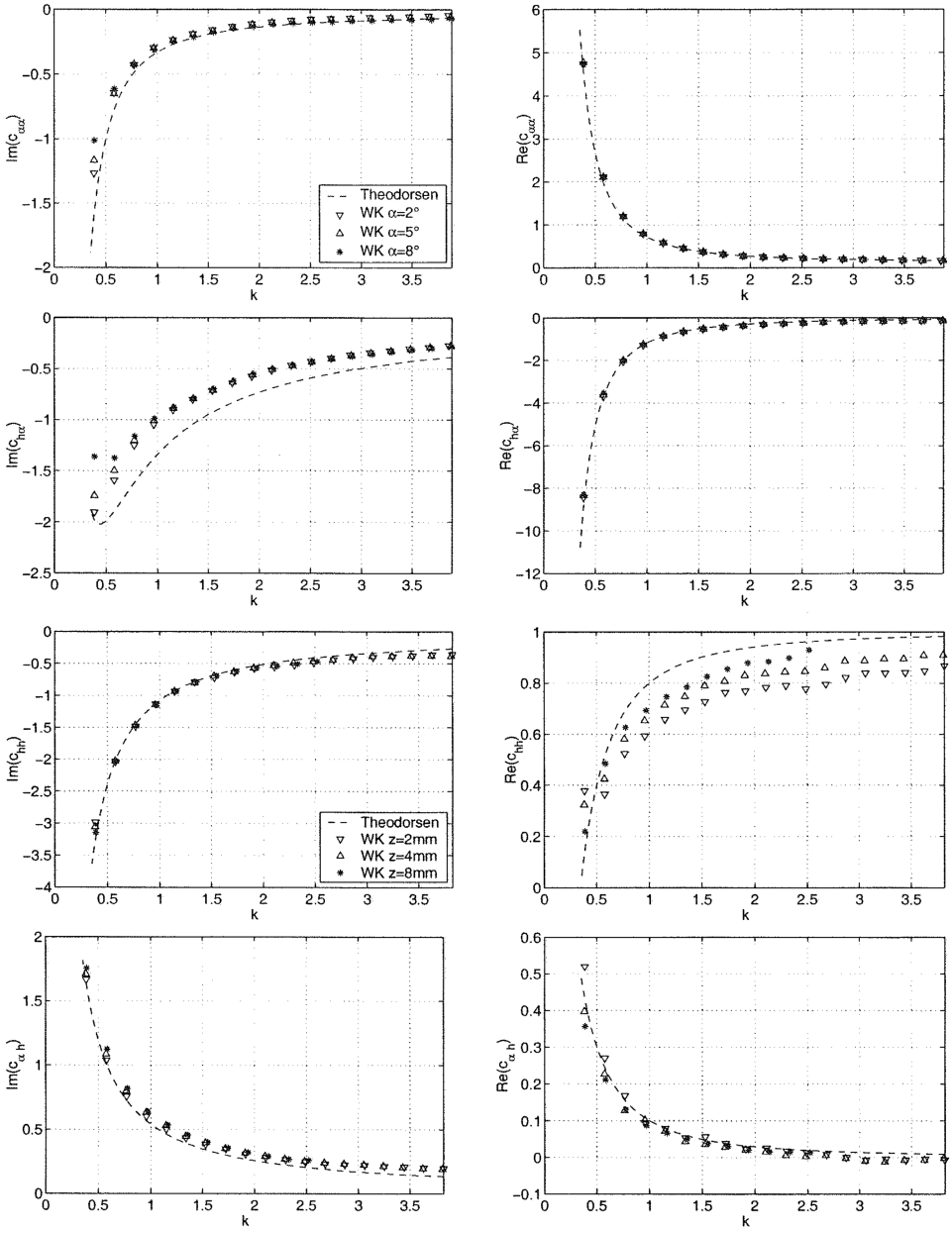

Fig. 6 Flutter derivatives for section M from water tunnel measurements

experimental results. In contrast, section R is a bluff section where the flutter derivative $c''_{\alpha\alpha}$ changes sign - an indication of torsional flutter. The critical wind speed is, as expectedly, lower than for section P. The difference between the numerical and experimental results highlights the shortcomings of the CFD method for bluff sections.

The open section G shows the best aerodynamic performance. For all structural data sets, the critical wind speed is the highest amongst the tested sections. However, the discrepancies between

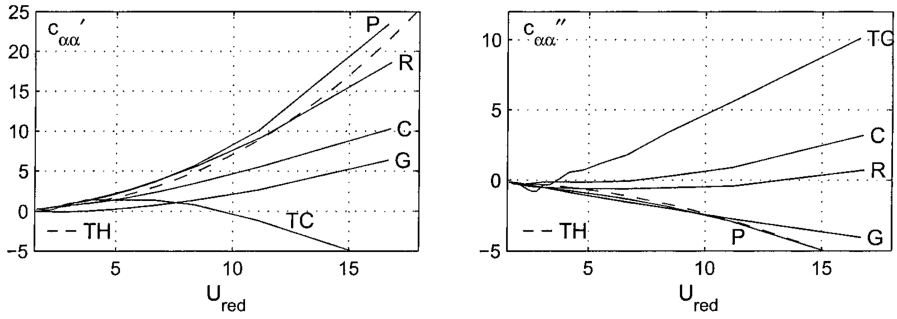

Fig. 7 Comparison of flutter derivatives obtained from water tunnel measurements, TH = analytical solution for a flat plate

CFD and experimental results are large, with the CFD method underestimating the critical wind speed. This seems to be due to the numerical difficulties the CFD method faces for sections where a separation and re-attachment of the flow can occur. A CFD analysis does not seem to be suitable for open sections. In addition, the analytical method can not be used so that for open sections experimental tests are the only reliable means.

The sections TC and C show the worst aerodynamic performance. The derivative $c''_{\alpha\alpha}$ of section TC crosses from negative to positive at a very low reduced wind speed. The observed flutter was a pure torsional one. The effect of the vertical vibration on the flutter instabilities was negligible. The difference between numerical and experimental results is large for section C whereas for section TC a difference is not apparent, except for the structural data set 4.

In general, the numerical results for streamlined section are in good agreement with the experimental results. For bluff and open sections, the CFD method seems less accurate.

The effect of different amplitudes was also tested but found to be negligible except for the bluff section TC where differences of 25% were observed for an amplitude range of 2° to 8°.

5.2. Further studies

5.2.1. Effective angle of attack

The angle at which the wind attacks the bridge influences the critical wind speed for flutter. Angles as small as 1° can have a significant impact on the magnitude of the critical wind speed. It is therefore common practice to assess the dynamic behaviour of the bridge for a range of angles of attack. However, the investigations must also consider the so-called effective angle of attack, particularly if the wind tunnel experiments are undertaken with the free vibration method (Starossek 1992).

The effective angle of attack τ_{eff} is the angle of wind incidence τ plus the static rotation of the bridge deck α^s that is induced by the wind (and around which the rotational vibration $\alpha(t)$ occurs). For horizontal wind ($\tau = 0$), the effective angle of attack consists only of the static rotation, i.e., $\tau_{eff} = \alpha^s$. This case is referred to in Fig. 10.

A static rotation is caused when the resultant of the drag and lift forces is eccentric to the shear centre of the bridge deck. The static moment coefficient is usually nonzero. For a section whose top and bottom portions are asymmetrical to each other, this statement even holds for horizontal flow. The ensuing static aerodynamic moment leads to a static rotation of the bridge deck that in turn

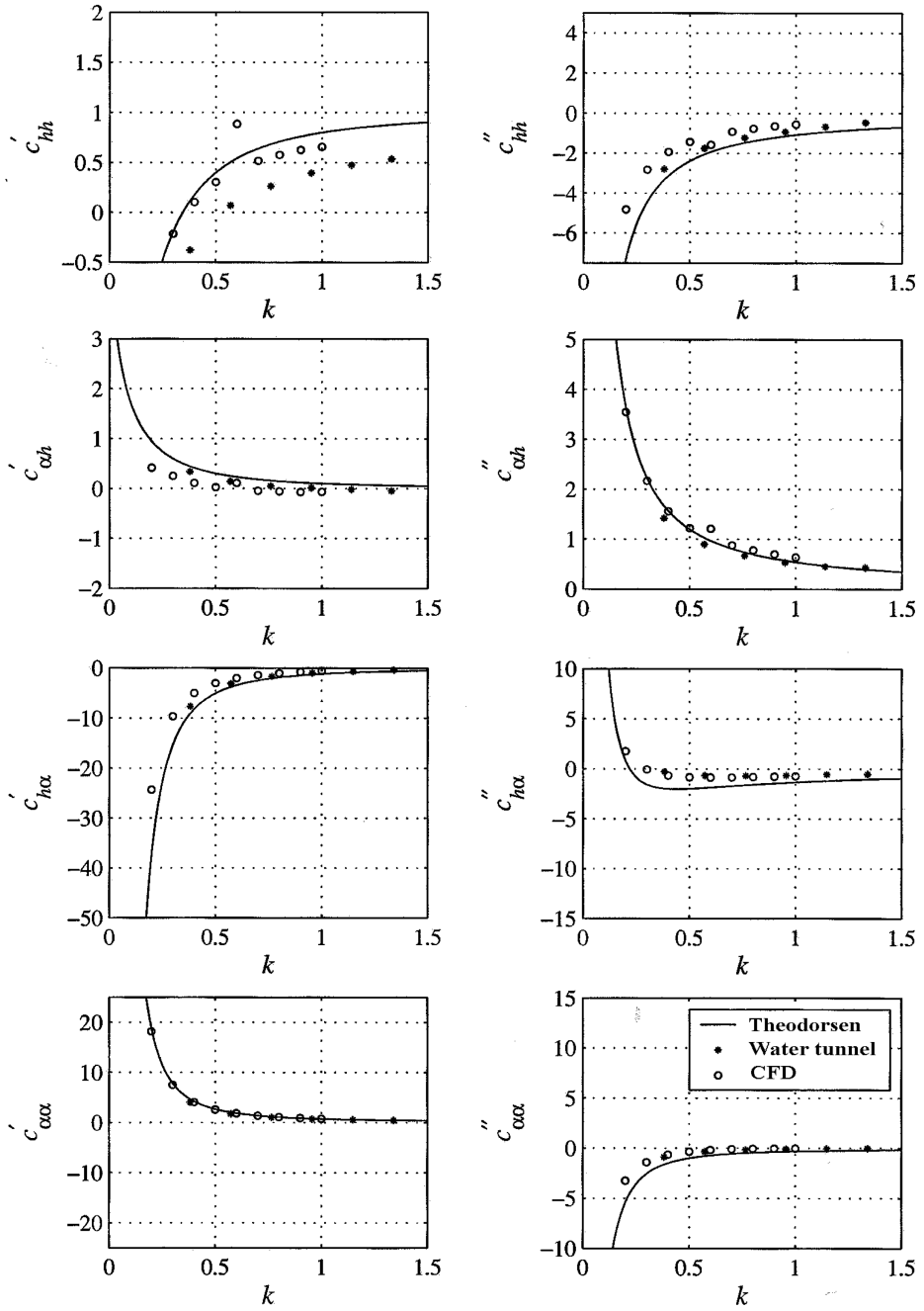

Fig. 8 Comparison of flutter derivatives for section GB obtained from experiments and numerical simulations

results in an effective angle of attack. The latter depends not only on the aerodynamic forces acting on the section, which vary with τ_{eff}, but also on the torsional stiffness of the structure. Therefore, more flexible systems can still be exposed to a significant effective angle of attack even if the static moment coefficient is small.

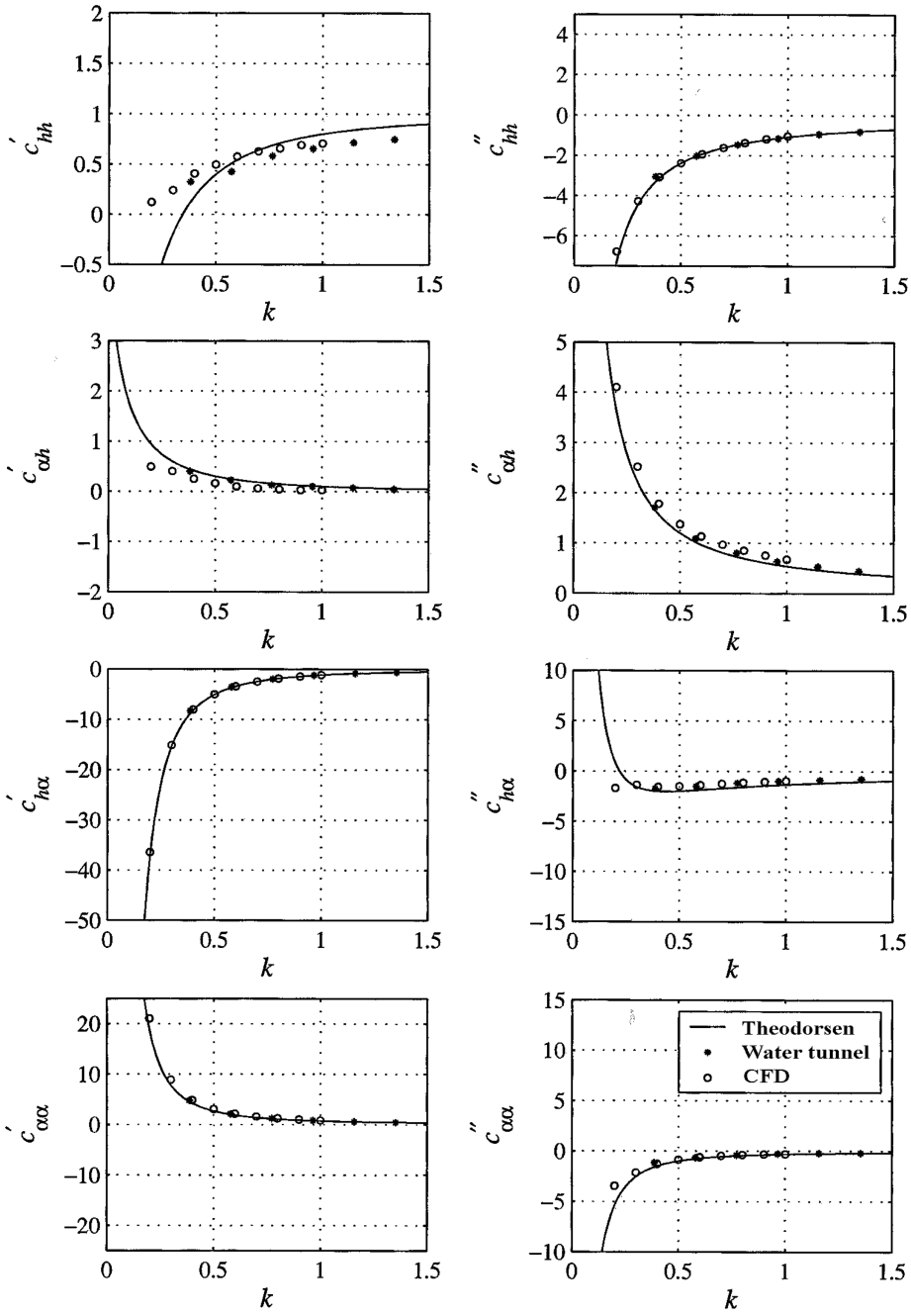

Fig. 9 Comparison of flutter derivatives for section M obtained from experiments and numerical simulations

Closed-form expressions can be derived for the wind-induced static rotation and the effective angle of attack (Starossek 1992). For sake of simplicity, horizontal wind is assumed in the following. When using a linearised static moment coefficient $C_M(\alpha)$, the static aerodynamic moment is

Table 4 Critical wind speeds [m/s] for flutter for various sections and four structural data sets

		1	2	3	4
Section	Method	u_{crit}	u_{crit}	u_{crit}	u_{crit}
GB	numerical	21.5	40.2	73.0	15.5
	experimental	20.6	41.3	70.2	16.1
S	numerical	25.3	48.0	85.6	31.5
	experimental	21.4	42.5	72.1	18.4
M	numerical	20.0	39.8	67.6	22.0
	experimental	19.2	39.4	65.5	16.7
P	numerical	18.7	36.9	63.5	22.8
	experimental	19.7	38.3	66.4	20.2
R	numerical	11.1	26.7	41.5	19.3
	experimental	15.6	34.8	55.6	16.3
B8	numerical	18.4	36.2	63.6	21.8
	experimental	18.0	37.9	63.1	16.6
C	numerical	12.0	25.4	45.7	14.8
	experimental	8.0	19.7	29.0	15.3
TC	numerical	7.4	20.0	29.8	14.6
	experimental	7.4	19.4	29.0	22.5
G	numerical	32.1	60.0	110.4	34.0
	experimental	45.8	76.2	163.4	43.9
flat plate	analytical	22.1	43.1	74.5	25.0

Table 5 Critical reduced frequencies for flutter for various sections and four structural data sets. Ratio is defined as numerical k_{crit} divided by experimental k_{crit}

		1		2		3		4	
Section	Method	k_{crit}	ratio	k_{crit}	ratio	k_{crit}	ratio	k_{crit}	ratio
GB	numerical	0.27	0.93	0.37	1	0.26	0.93	0.96	1.04
	experimental	0.29		0.37		0.28		0.92	
S	numerical	0.22	0.81	0.26	0.79	0.18	0.72	0.43	0.55
	experimental	0.27		0.33		0.25		0.78	
M	numerical	0.3	0.97	0.37	0.97	0.29	0.97	0.66	0.76
	experimental	0.31		0.38		0.3		0.87	
P	numerical	0.32	1.07	0.4	1.05	0.31	1.07	0.63	0.89
	experimental	0.3		0.38		0.29		0.71	
R	numerical	0.56	1.4	0.6	1.33	0.57	1.43	0.75	0.83
	experimental	0.4		0.45		0.4		0.9	
B8	numerical	0.33	0.97	0.42	1.02	0.33	0.97	0.66	0.75
	experimental	0.34		0.41		0.34		0.88	
C	numerical	0.54	0.67	0.67	0.77	0.54	0.61	0.99	1.02
	experimental	0.81		0.87		0.89		0.97	
TC	numerical	0.89	1.01	0.9	1.02	0.88	1.01	0.97	1.52
	experimental	0.88		0.88		0.87		0.64	
G	numerical	0.17	1.31	0.21	1.17	0.14	1.27	0.4	1.21
	experimental	0.13		0.18		0.11		0.33	
flat plate	analytical	0.26		0.33		0.25		0.58	

Table 6 Numerically determined critical wind speeds in comparison with experimental results by Larsen and Jacobsen (1992)

Section	u_{crit}(exp)/u_{crit}(Selberg)	u_{crit}(num)/u_{crit}(Selberg)
GB	0.99	0.98
B2	1.04	1.02
B3	1.11	1.01
B4	1.00	0.99
B5	1.03	0.98
B6	1.05	0.99
B7	1.03	0.97

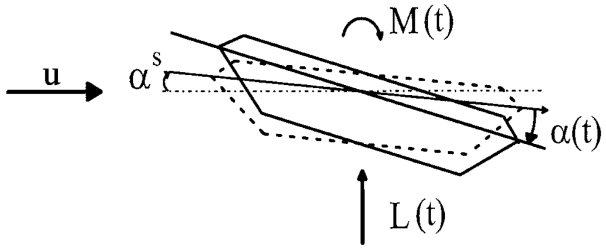

Fig. 10 Static rotation and effective angle of attack

$$M^s = \left(C_{M_0} + \frac{dC_M}{d\alpha}\alpha\right) q(2b)^2, \tag{14}$$

where $q = \frac{1}{2}\rho u^2$ is the dynamic pressure. The static equilibrium condition for the rotational degree of freedom reads

$$M^s - k_\alpha \alpha^s = 0 \tag{15}$$

where k_α is the rotational stiffness coefficient. Substituting the linearised aerodynamic moment expression into the equilibrium condition and solving for the static rotation leads to

$$\alpha^s = \frac{C_{M_0} q(2b)^2}{k_\alpha - \frac{dC_M}{d\alpha} q(2b)^2} \tag{16}$$

which can be rewritten as

$$\alpha^s = \frac{C_{M_0}}{\frac{\pi}{2}\left(\frac{u^{div}}{u}\right)^2 - \frac{dC_M}{d\alpha}} \tag{17}$$

where $u^{div} = r\sqrt{\mu}\omega_\alpha b$ is the analytically derived critical wind speed for static divergence of a flat plate. Because horizontal wind is assumed, the static rotation thus determined equals the effective angle of attack.

The results for the nine sections, using the structural parameters from data set 1 in Table 1 and a

Table 7 Effective angle of attack for u=22 m/s and structural data set 1

Section	cM	dcM/da	t_{eff} [degree]
R	0.004	0.7964	0.05
M	0.036	1.5928	0.56
GB	0.033	1.1516	0.48
S	0.026	1.335	0.39
G	0.014	0.6474	0.18
TC	-0.005	-9.1673	-0.02
C	0.086	0.5787	1.09
P	0.002	1.7418	0.03
B8	0.083	1.2319	1.23

wind speed of $u = 22$ m/s, are shown in Table 7. The largest effective angle of attack was determined for section B8. Further investigation showed that section B8 is particularly prone to aerodynamic instability for increasing angle of attack. This also follows from the fact that the $c''_{\alpha\alpha}$ derivative turns positive for $\alpha \approx 1°$ (Fig. 11).

5.2.2. Non-critical vibrations

The flutter derivatives are only valid for harmonic motion. This condition is solely present at the onset of flutter, which is sufficient for the determination of the critical wind speed–the key parameter for an assessment of the aerodynamic stability of the bridge structure. Before and after the onset of flutter, the motion is non-harmonic due to positive or negative damping. The description of non-critical vibrations, which is particularly of interest for determining the aerodynamic performance of the structure at service, can still be accomplished with the use of Indicial Functions (Scanlan, *et al*. 1974) or the method of Rational Function Approximation (Karpel and Strul 1996). Both methods have their advantages and disadvantages in terms of accuracy and computational speed. In this study, Indicial Functions were used to describe non-critical vibrations in the time domain.

The numerically determined flutter derivatives c_{mn} for the sections were used to calculate the coefficients of the Indicial Functions by means of the Levenberg-Marquardt method. Once the coefficients were found, the time response of the vibration could be determined with the Predictor-Corrector method for a given set of structural data. Solutions for the GB section are shown in Fig. 12. For a wind speed of $u = 38$ m/s, it can be seen that the vibration is positively damped, and for a wind speed of $u = 45$ m/s, the amplitude is clearly divergent. For a wind speed of $u = 41$ m/s the amplitude is constant. The critical wind speed was determined in numerical simulations to be $u = 40.2$ m/s.

5.2.3. Lateral vibrations

Flutter analysis is generally based on a 2-DOF system that moves in the vertical and rotational directions. For a more accurate assessment, the lateral motion can be included. The self-induced aerodynamic drag force, in addition to the lift and moment forces in Eqs. (2) and (3), was suggested by Simiu and Scanlan (1996) to be described by

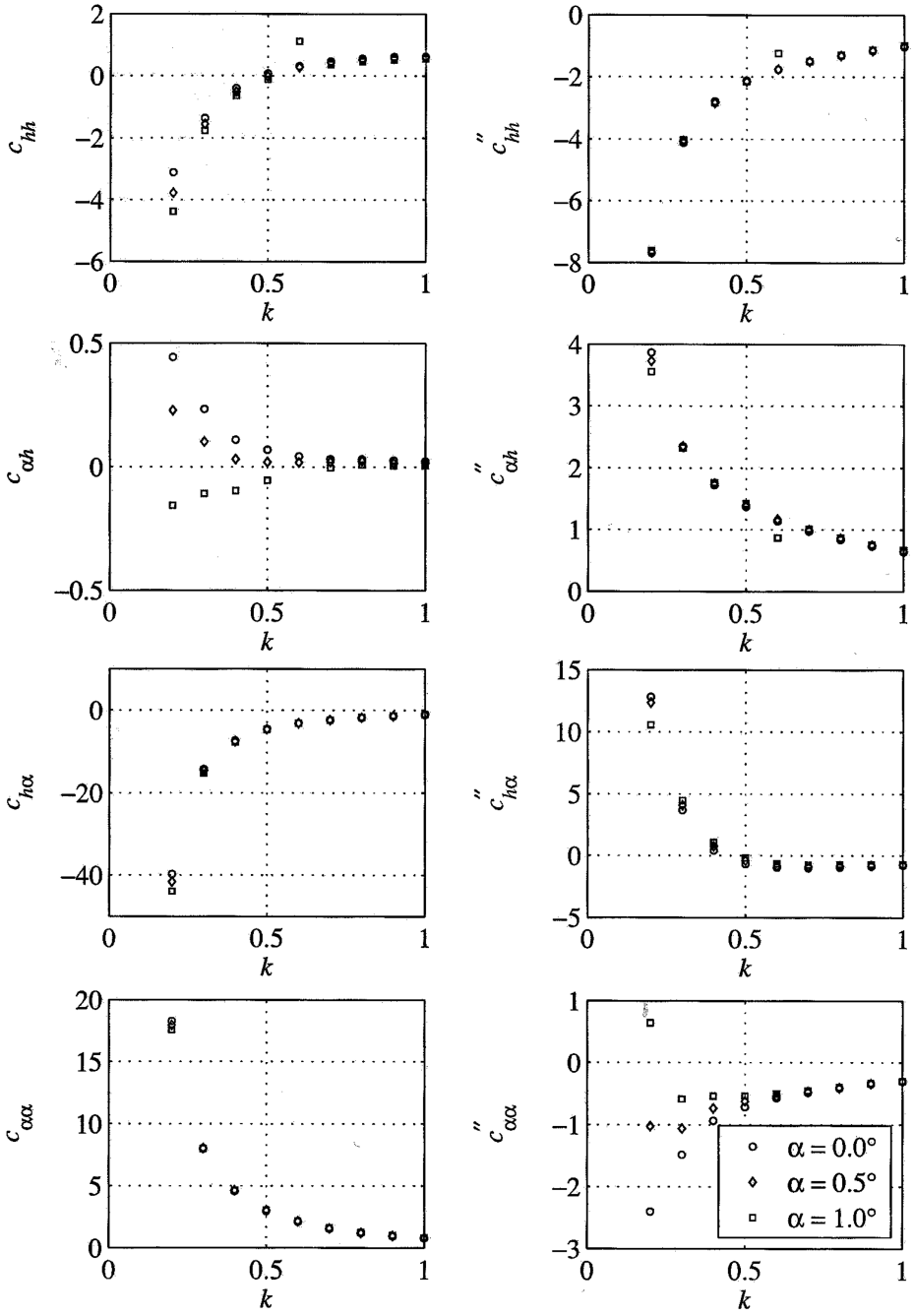

Fig. 11 Numerically obtained flutter derivatives for section B8 for various angles of attack

$$D = \frac{1}{2}\rho u^2 B\left(KP_1^*\frac{\dot{p}}{u} + KP_2^*\frac{B\dot{\alpha}}{u} + K^2P_3^*\alpha + K^2P_4^*\frac{h}{B}\right) \tag{18}$$

The validity of such a linear approach is questioned based on fundamental geometrical

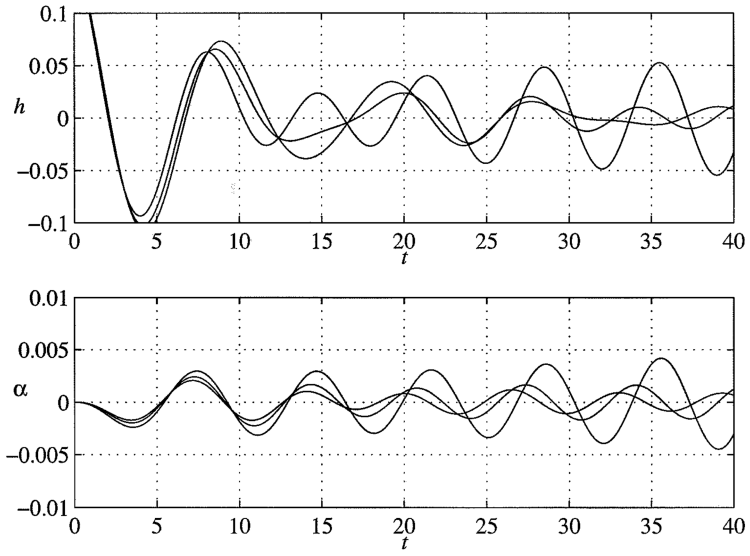

Fig. 12 Time domain simulation for section GB with wind speeds of $u = 38$ m/s (convergent), $u = 41$ m/s (constant), and $u = 45$ m/s (divergent amplitudes)

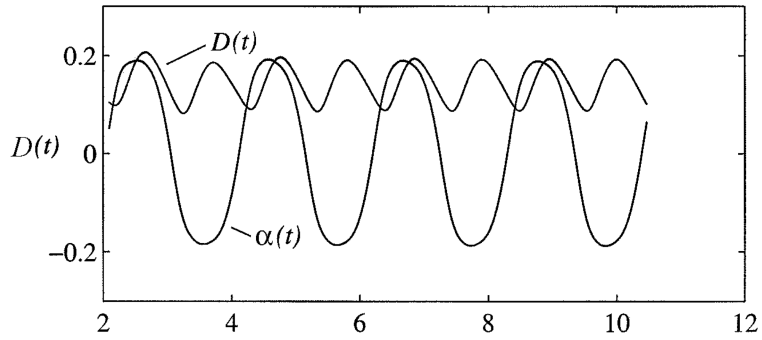

Fig. 13 Numerically obtained time history of drag force during rotational vibration

considerations and on the results of the numerical simulations. A positive rotation and the corresponding negative rotation result in the same exposed area for the wind to act on (at least when the top and bottom portions of the section are symmetrical to each other). Thus, the dynamic drag force (or a major part of it) can be expected to vary with twice the frequency of the rotational vibration. This expectation is corroborated by the time history of the drag force during rotational motion α(t) that was obtained from a numerical simulation (Fig. 13).

6. Conclusions

Flutter derivatives for nine different bridge deck sections were obtained from experiments undertaken in a water tunnel. The purpose was to provide a benchmark for the numerical

assessment of bridge deck flutter derivatives. Over 30 sections were studied numerically by using a commercially available CFD software package, which is based on the Finite Volume method. The results of the two methods and analytical solutions for a flat plate were compared with focus on the accuracy of the CFD code. Good agreement between the various solutions was found in certain cases, in particular, for streamlined closed sections. Further studies concerning the effective angle of attack, noncritical vibrations, and the effect of lateral motion were carried out. The full set of results from the experiments and the numerical simulations is available online to provide researchers and engineers with a comprehensive benchmarking tool for the evaluation of CFD code or for other purposes.

References

Flamand, O., de la Foye, A. and Danbo, F. (2001), "Aerodynamic Derivatives of Three Bridge Decks measured by the Forced Oscillation Technique", *Proc. of the 3rd European and African Conf. on Wind Engineering*, Eindhoven, Netherlands, 606-610.

Frauenhofer Institute (2008), *Mesh-based parallel code coupling interface: MpCCI*, Further information available online at http://www.mpcci.de.

Hortmanns, M. (1997), "Zur Identifikation und Berücksichtigung nichtlinearer aeroelastischer Effekte", *Dissertation*, RTWH Aachen, Lehrstuhl fur Stahlbau.

Karpel, M. and Strul, E. (1996), "Minimum state unsteady aerodynamic approximations with flexible constraints", *J. Aircraft*, **33**, 1190-1196.

Larsen, A. and Jacobsen, A.S. (1992), *Aerodynamic Design of the Great Belt East Bridge*, Aerodynamics of Large Bridges, A.A. Balkema.

Larsen, A. and Walther, J. (1998), "Discrete Vortex Simulation of Flow around Five Generic Bridge Deck Sections", *J. Wind Eng. Ind. Aerod*., **77-78**, 657-672.

Larsen, A. and Astiz, M. (1998), *Aerodynamic Considerations for the Gibraltar Feasibility Study*, Bridge Aerodynamics, A.A. Balkema.

Morgenthal, G. (2002), "Aerodynamic Analysis of Structures using High-Resolution Vortex Particle Methods", PhD Thesis, Dep. of Eng., University of Cambridge.

Reinhold, T.A., Brinch, M. and Damsgaard, A. (1992), *Wind tunnel tests for the Great Belt Link*, Aerodynamics of Large Bridges, 1135-1150.

Scanlan, R. and Tomko, J. (1971), "Airfoil and Bridge Deck Flutter Derivatives", *J. Eng. Mech. Div.*, 97-EM6, 1717-1737.

Scanlan, R.H., Beliveau, J.G. and Budlong, K.S. (1974), "Impulse aerodynamic functions for bridge decks", *J. Eng. Mech. Div.* ASCE, 100-EM4, 657-672.

Simiu, S. and Scanlan, R.H. (1996), *Wind Effects on Structures*, 3rd ed., John Wiley and Sons, New York.

Starossek, U. (1992), *Brückendynamik - Winderregte Schwingungen von Seilbrücken*, Friedr. Vieweg & Sohn, Braunschweig/Wiesbaden (in German). Available online at http://www.starossek.de.

Starossek, U. (1993), "Prediction of bridge flutter through use of finite elements", *Struct. Eng. Rev.*, **5**(4), 301-307. Available online at http://www.starossek.de.

Starossek, U. (1998), "Complex notation in flutter analysis", *J. Struct. Eng.* ASCE, **124**(8), 975-977 (Discussion and Closure in **125**(10), 1199-1200).

Starossek, U. (2009), *Flutter derivatives for various sections obtained from experiments and numerical simulations*, Hamburg University of Technology, data files. Available online at http://www.starossek.de.

Theodorsen, T. (1935). "General theory of aerodynamic instability and the mechanism of flutter", National Advisory Committee for Aeronautics, Technical Report No. 496, 413-433.

Thiesemann, L. and Starossek, U. (2002), "Numerical evaluation of flutter derivatives", *Proc. of 4th Int. on Structural Dynamics-EURODYN2002*, Munich, Germany, Sept. 2-5, 2002, Balkema, Lisse, 1561-1566.

Thiesemann, L. (2007), "Zur Ermittlung von Flatterderivativa aus Versuchen und mittels numerischer

Strömungsmechanik", Dr.-Ing. Thesis, Hamburg University of Technology (in German). Available online at http://www.sh.tu-harburg.de/index.html.

Walther, J.H. (1994), "Discrete Vortex Method for Two-dimensional Flow past Bodies of Arbitary Shape Undergoing Prescribed Rotary and Translational Motion", PhD Thesis, Department of Fluid Mechanics, Technical University of Denmark.

Wienand, B. (1994), *Experimentelle und rechnerische Untersuchung der aerodynamischen Stabilität weitgespannter Brücken unter Berücksichtigung nichtlinearer Windkräfte*, Fachbereich Bauingenieurwesen der Universität Kassel.

JH